The Vinblastine Binding Site Adopts High- and Low-Affinity Conformations during a Transport Cycle of P-glycoprotein†

Catherine Martin,‡ Christopher F. Higgins,§ and Richard Callaghan*,‡

Nuffield Department of Clinical Laboratory Sciences, University of Oxford, John Radcliffe Hospital, Oxford OX3 9DU, U.K., and MRC Clinical Sciences Centre, Imperial College School of Medicine, Hammersmith Hospital, London W12 0NN, U.K.

Received June 12, 2001; Revised Manuscript Received August 30, 2001

ABSTRACT: Conceptually one may envisage that substrate binding sites on the ABC transporter P-gp cycle between high- and low-affinity conformations in response to signals arising from nucleotide hydrolysis to effect active transport. A radioligand binding assay was used to characterize the interaction of [^{3}H]vinblastine with P-gp and determine how drug binding site parameters are altered during a catalytic cycle of P-gp. In the absence of nucleotide, we show that [^{3}H]vinblastine interacts with a single class of binding site with high affinity ($K_d = 80 \pm 18$ nM). In the presence of the nonhydrolyzable ATP analogue AMP-PNP, the drug binding site was in a low-affinity conformation, manifest by a 9-fold increase in K_d ($K_d = 731 \pm 20$ nM). There was no alteration in the binding capacity, reflecting a complete shift in the high-affinity site to a low-affinity form. The posthydrolytic (Mg·ADP·V_i bound) form of P-gp also exhibited low-affinity substrate binding ($K_d = 446 \pm 57$ nM). Restoration of the high-affinity drug binding site conformation ($K_d = 131 \pm 32$ nM) did not occur until release of phosphate from the posthydrolysis P-gp·Mg·ADP·P_i. complex. Our results suggest that alteration of the affinity of the vinblastine binding site involves only one nucleotide binding domain per transport cycle. The binding of ATP provides the signal to instigate this change, while release of phosphate post-ATP hydrolysis returns the transporter to its original state to complete the cycle.

P-glycoprotein (P-gp)[1] is an integral membrane protein and member of the *A*TP *b*inding *c*assette (ABC) superfamily of transporters. This transporter, whose normal cellular role is not yet clear, has been implicated in conferring multidrug resistance (MDR) in many tumor types. Overexpression of P-gp leads to reduced intracellular levels of myriad chemically and functionally diverse cytotoxic drugs in tumors, thereby reducing their efficacy in cancer chemotherapy. The molecular basis of P-gp's broad substrate specificity is the presence of multiple drug recognition sites within its transmembrane domains (TMDs) (*1*−*3*). However, the mechanism of P-gp-mediated drug efflux has yet to be understood.

P-gp effects translocation of drug by coupling the energy derived from ATP hydrolysis at its nucleotide binding domains (NBDs) to solute movement. However, there is scant knowledge at best concerning the mechanisms that transduce signals generated from binding of substrate at the TMDs into hydrolysis of ATP at the NBDs or about the type of signaling transmitted back to the binding site as the protein undergoes a catalytic cycle. It is generally assumed that cycling of the drug site from high- to low-affinity states is driven by conformational changes and that this facilitates movement of drug across the membrane.

There is growing evidence that communication between domains on P-gp is via conformational changes. For instance, binding of drugs at the TMDs has been shown to quench the fluorescent probe MIANS, covalently bound at the NBDs (*4*). Communication in the opposite direction has been demonstrated by the ability of nucleotide binding and hydrolysis within the NBDs to elicit conformational changes as shown by alterations in tryptophan quenching (*5*, *6*), differential trypsin digestion profiles (*7*, *8*), and changes in the accessibility of the extracellular epitope for the UIC2 antibody (*9*).

The consequences of nucleotide-induced conformational changes for drug binding have not yet been fully elucidated. Radioligand and photoaffinity labeling studies have shown reduced binding of the substrates vinblastine and iodoarylazidoprazosin (IAAP) (*10*−*12*) when protein is trapped by vanadate in a posthydrolysis conformation. Furthermore, we have previously shown that binding of nucleotide, prior to hydrolysis, triggers conformational alteration of the drug binding site as manifested by a reduction in the binding capacity of [^{3}H]vinblastine (*10*). Drug binding was recovered following completion of a catalytic cycle. The observed reduction in binding capacity may be due to either an occlusion of the high-affinity binding site or a switch in its properties from a high- to a low-affinity site. In the previous

† This work was supported by Cancer Research Campaign Program Grant ARG/CS SP1861/0301 and the Imperial Cancer Research Fund.

* To whom correspondence should be addressed. E-mail: richard.callaghan@ndcls.ox.ac.uk. Facsimile: +44 1865 221 834. Telephone: +44 1865 221 110.

‡ University of Oxford, John Radcliffe Hospital.

§ Imperial College School of Medicine, Hammersmith Hospital.

[1] Abbreviations: ABC, ATP binding cassette transporter family; P-gp, P-glycoprotein; NBD, nucleotide binding domain; AMP-PNP, 5′-adenylyl imidodiphosphate; K_d, affinity binding constant; B_{max}, binding capacity.

10.1021/bi011211z CCC: $20.00 © 2001 American Chemical Society
Published on Web 12/01/2001

investigation we were unable to distinguish between these two possibilities since the highest achievable [^{3}H]vinblastine concentration was only 100 nM, thereby precluding detection of low-affinity binding.

We have now developed a mixed homologous saturation radioligand saturation assay to enable investigation of P-gp with the transported substrate vinblastine at several discrete stages of the catalytic cycle, over a wide concentration range of vinblastine. The data provide a mechanistic understanding of the transport process by elucidating the link between the ATP catalytic cycle and drug binding events.

EXPERIMENTAL PROCEDURES

Materials. Disodium adenosine triphosphate (Na_2ATP), sodium orthovanadate, and 5′-adenylyl imidodiphosphate (AMP-PNP) were purchased from Sigma (Poole, U.K.). [^{3}H]Vinblastine sulfate (11−12 Ci/mmol) and Sephadex G-50 (fine) resin were obtained from Amersham Pharmacia Biotech (Amersham, U.K.). 8-Azido[α-^{32}P]ATP (2−10 Ci/mmol) and 8-azidoATP were from ICN Pharmaceuticals BV, The Netherlands.

Cell Lines and Plasma Membrane Preparation. The P-gp overexpressing drug-resistant Chinese hamster ovary cell line (CH^RB30) was routinely cultured as previously described (*13*). In brief, cells were grown at 37 °C in α-minimal essential growth medium supplemented with 30 μg mL^{-1} colchicine. Plasma membrane vesicles were prepared by disruption of intact cells by N_2 cavitation and collected by sucrose density centrifugation as described (*14*). Membrane vesicles were stored at protein concentrations of 20 mg mL^{-1} at −80 °C in buffer 1 containing 250 mM sucrose, 10 mM Tris-HCl (pH 7.4), and the protease inhibitors leupeptin (0.1 mg mL^{-1}), pepstatin A (0.1 mg mL^{-1}), and benzamidine (1 mM).

Equilibrium Radioligand Binding to CH^RB30 Membrane Vesicles. The equilibrium binding of [^{3}H]vinblastine was measured using a combination of saturation and homologous binding displacement to investigate binding parameters over a wider ligand concentration range than has previously been possible. All binding studies were done in a total reaction volume of 100 μL of buffer 2 containing 50 mM Tris-HCl, pH 7.4. Binding equilibrium was reached following a 2.5 h incubation at 22 °C. Samples were filtered rapidly under vacuum through GF/F glass fiber filters to separate bound and unbound ligand. After being washed twice with 3 mL of buffer 3 (20 mM Tris-HCl, pH 7.4, 20 mM $MgSO_4$), radioactivity trapped on the filter was measured by liquid scintillation counting. Nonspecific binding was measured in the presence of excess nicardipine (10 μM) and was subtracted from all values. CH^RB30 membranes (15 μg) were incubated with different concentrations of radioligand up to 100 nM to measure binding at low radioligand concentrations (saturation isotherm assay). Binding at higher ligand concentrations was measured by incubating membranes with a fixed concentration of labeled ligand (100 nM) and increasing concentrations of unlabeled ligand up to 3 μM (homologous displacement assay). The validity of combining these data in a mixed homologous saturation assay to measure binding over a wider range of ligand concentration has been discussed elsewhere (*15*−*17*). To determine the amount of vinblastine bound specifically at the higher vinblastine concentration range, the dilution of the specific activity of the radioligand at each concentration of unlabeled ligand was taken into account. Specific binding (picomoles per milligram) was plotted as a function of ligand concentration. The data were fitted with two different equations that reflect distinct pharmacological scenarios. Equation 1 is a dose−response relationship for a single class of drug binding site as derived by Waud (*18*):

$$Y = \frac{[L]}{K_d + [L]} \quad (1)$$

where Y is the fraction of radioligand bound (amount bound/binding capacity), [L] is the log of molar vinblastine concentration (M), and K_d is the binding dissociation constant (M). The Adair equation (eq 2) was used to determine whether binding data could be fitted by an equation describing two independent sites of different affinity for radioligand (*19*):

$$Y = \frac{K_{d2}[L] + 2[L]^2}{2(K_{d1}K_{d2} + K_{d2}[L] + [L]^2)} \quad (2)$$

Y = fraction of radioligand bound, [L] is the log of molar vinblastine concentration (M), and K_{d1} and K_{d2} are the dissociation constants for vinblastine binding to two independent sites.

Scatchard analysis was also employed by plotting the specific bound/[vinblastine] as a function of bound and fitted by linear regression with the equation:

$$\frac{B}{[L]} = \frac{B_{max}}{[L]} - \frac{B}{K_d} \quad (3)$$

B is the amount of specific [^{3}H]vinblastine bound (pmol/mg), B_{max} is the maximal binding capacity (pmol/mg), [L] is the free vinblastine concentration, and K_d is the dissociation constant for vinblastine.

Theoretical Curve Generation. Theoretical curves were generated to simulate pharmacological scenarios involving interaction of drug with a single class of site or to two independent sites of different affinity. Curves were generated using the dose−response equation (eq 1) where the fraction bound was determined over a range of ligand concentrations with different values for affinity, arbitrarily beginning with a K_d = 1 nM. The Adair equation (eq 2) was used to generate a series of curves where the fraction of ligand bound was measured over a range of ligand concentrations where the ratio of the difference in the value of K_{d1} and K_{d2} increases. K_{d1} was arbitrarily set at 1 nM for the simulations.

All of the curve fitting was carried out using nonlinear regression analysis using Graphpad Prism 3.0 (GraphPad software, San Diego, CA). The goodness of fit of the data to the complex model versus the simpler model was achieved by comparing the sum of squares for each fit using the *F*-test, which also takes the number of model parameters and data points into consideration. The complex model was only used where a P value of ≤0.05 was obtained. Unpaired Student's *t* test was used to statistically compare sample means. In all cases, a P value of ≤0.05 was considered statistically significant.

Measurement of ATPase Activity in CH^{R}B30 Membranes. ATPase activity of P-gp was detected by following the release of inorganic phosphate using a colorimetric assay based on a modification of the assay first described by Chifflet (*20*). Membrane vesicles or proteoliposomes (1 μg) were incubated in buffer 4 (150 mM NH_4Cl, 50 mM Tris-HCl, pH 7.4, 5 mM $MgSO_4$, 0.02% NaN_3) in the presence of 0−2.5 mM Na_2ATP and 50 μM verapamil over a 20 min period at 37 °C. Drug-stimulated ATPase activity was plotted as a function of ATP concentration using the Michaelis−Menten equation:

$$Y = \frac{V_{max}[S]}{K_d + [S]} \quad (4)$$

Y is ATPase activity (nmol min^{-1} mg^{-1}), V_{max} is maximal activity (nmol min^{-1} mg^{-1}), [S] is ATP concentration (mM), K_m is the concentration of ATP (mM) which produces 50% of the maximal activity.

Vanadate Trapping of P-gp. Membrane vesicles (4 μg/μL) were incubated with 2 mM Na_2ATP or 8-azidoATP, 0.3 mM $NaVO_3$, 50 μM verapamil, and buffer 4 in a total volume of 400 μL over a 20 min period at 37 °C. Sodium orthovanadate stock solutions (100 mM) were adjusted to pH 10 and boiled for 2−5 min to eliminate all polymeric species present (*21*) prior to each use. The reaction was stopped by placing the samples on ice followed by centrifuging 120 μL aliquots through 1 mL Sephadex G-50 spin columns at 1000*g* to remove unbound components. Where 8-azidoATP was used in the trapping experiments, 20% (v/v) glycerol was included in buffer 4, and the azido nucleotide was cross-linked to the protein by placing samples on ice and exposing to UV lamp (100 W) at a distance of 5 cm for 4 min, prior to applying samples to spin columns. [^{3}H]Vinblastine binding assays involving vanadate-trapped protein were done in buffer 2 supplemented with 100 μM sodium orthovanadate. This concentration has previously been shown to be sufficient to prevent breakdown of the P-gp·ADP·V_i complex (*10*).

Purification and Reconstitution of P-gp from CH^{R}B30 Membranes. P-gp was purified from CH^{R}B30 membranes by first solubilizing the protein in buffer 5 (5 mM PIPES, 0.5 mM EDTA, 0.02% NaN_3, pH 7.1) containing 1% (w/v) dodecyl maltoside in the presence of 0.4% (w/v) crude lipid mixture (soybean asolectin) at a protein concentration of 3−5 mg mL^{-1}. The soluble fraction was harvested by ultracentrifugation at 100000*g* for 30 min in a TLA100 rotor. Anion-exchange chromatography was then used to purify P-gp from the soluble protein fraction to approximately 60% homogeneity as described previously (*22*). Reconstitution of purified P-gp was achieved using SM-2 Bio-Beads to remove detergent from protein/lipid/detergent mixtures as described in detail elsewhere (*23*). Briefly, large unilamellar vesicles comprising phosphatidylcholine (PC) and phosphatidylethanolamine (PE) in a molar ratio of 9:1 were saturated with decyl maltoside. An aliquot of saturated lipid vesicles was added to solubilized P-gp to give a lipid:protein ratio of 3:1(w/w). The detergent/lipid/protein mixture was allowed to equilibrate on ice for 40 min prior to Bio-Bead additions (5 × 40 mg mL^{-1}). The efficiency of reconstitution was determined from the relative migration of protein and lipid through sucrose density gradients as described previously (*24*).

Photoaffinity Labeling of Reconstituted P-gp with 8-Azido-[α-^{32}P]ATP. Proteoliposomes (8 μg of protein) were incubated with 2 μM 8-azido[α-^{32}P]ATP (2−10 Ci/mmol) in buffer 4 in the presence of increasing concentrations of unlabeled 8-azidoATP (0−300 μM). Reactions were in a final volume of 70 μL and were incubated for 15 min at 37 °C. Labeling was stopped by placing the samples on ice. Bound nucleotide was cross-linked to the protein by UV-irradiating samples (100 W) for 4 min on ice at a distance of 5 cm. Unbound nucleotide was removed by trichloroacetic acid precipitation of P-gp followed by electrophoresis on 8% SDS−PAGE gels. The relative labeling efficiency of the samples was measured by autoradiography of the gels. The relative amount of 8-azido[α-^{32}P]ATP bound to the protein was plotted as a function of ATP concentration and the potency of the latter to displace the former obtained by curve fitting with the general dose−response equation:

$$Y = B_{min} + \frac{B_{max} - B_{min}}{1 + [L]/EC_{50}} \quad (5)$$

B_{min} and B_{max} are the minimum and maximum levels, respectively, of 8-azido[α-^{32}P]ATP bound, [L] is the amount of ATP added, and EC_{50} is the concentration of ATP required to displace half of the maximal 8-azido[α-^{32}P]ATP bound.

RESULTS

The aim of this study was to describe the mechanistic link between drug binding sites in the transmembrane domains and nucleotide interaction at the NBDs during a catalytic cycle of P-gp. To achieve this, radioligand binding studies have been used to directly measure the interaction of [^{3}H]vinblastine (a transported substrate of P-gp) with its binding site during four discrete stages of the catalytic cycle, namely, (1) prenucleotide binding, (2) when nucleotide is bound, (3) postnucleotide hydrolysis, and (4) following release of inorganic phosphate.

Our initial aim was to determine whether P-gp has a single binding site for [^{3}H]vinblastine. Alternatively, [^{3}H]vinblastine may bind to the protein at two distinct locations, which display different binding affinities. Such spatially *distinct* locations of dissimilar affinities are referred to as different classes of binding site. To determine the number of different classes of binding site, nonlinear curve fitting of experimental vinblastine binding to P-gp will be analyzed using two different equations. To illustrate their applicability, theoretical dose−response curves were generated using either eq 1, which described binding to a single class of binding site (Figure 1a), or the Adair equation (eq 2), which describes interaction at two independent sites of different affinity (Figure 1b). For instance, if the affinity of vinblastine binding to P-gp was reduced during the catalytic cycle, the binding curve as described by eq 1 would undergo a parallel shift to the right (Figure 1a). In contrast, if vinblastine interacted with two classes of site, the shape of the binding curve would be affected. For example, the slope of the linear portion of the curve would be altered, and at higher differences between

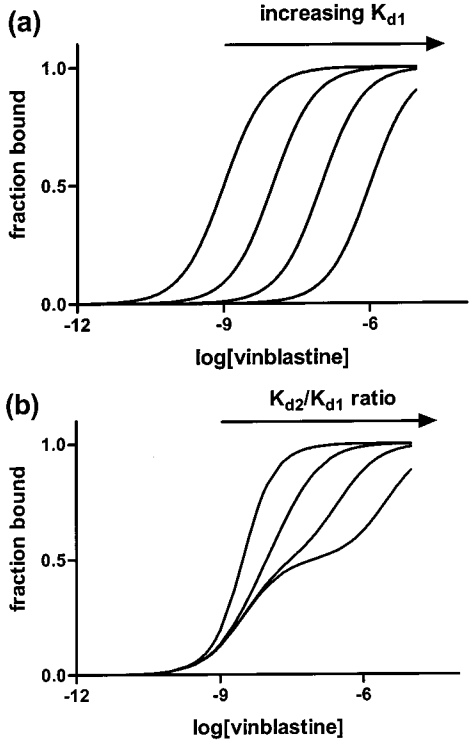

FIGURE 1: Theoretical binding curves were generated to demonstrate characteristics of binding to a single site or two independent sites of different affinity. (a) Dose−response curves as first described by Waud (eq 1 in Experimental Procedures) were produced by simulating the fraction of ligand bound to a single site over a range of ligand concentration having arbitrary affinity (K_{d1}) between 1 and 1000 nM. (b) Fraction of ligand bound to two independent sites determined over a range of ligand concentration where the ratio of the affinities of the two sites (K_{d2}/K_{d1}) is increased from 1 to 1000. An arbitrary value of $K_{d1} = 1$ nM was used, and data were modeled using the Adair equation as described in Experimental Procedures.

the two respective affinities (K_{d1} and K_{d2}), the curve would become biphasic as illustrated in Figure 1b. Both of these manifestations would be apparent in curve fitting to experimental data. It is important to note that this analysis cannot assign the stoichiometry of vinblastine binding to P-gp since multiple sites of a distinct class may be present on the protein. However, this analysis also has the capability to monitor the change in affinity of a single class of vinblastine binding site during a catalytic cycle.

Characteristics of [^{3}H]Vinblastine Binding to P-gp: Absence of Nucleotide. Figure 2a demonstrates a typical "saturation isotherm" for specific and nonspecific vinblastine binding to CH^{R}B30 membranes containing P-gp. The major limitation of this assay, which employs only radiolabeled vinblastine, is that concentrations of approximately 200 nM represent the upper limit. Given that the K_d for [^{3}H]vinblastine binding has been reported as approximately 50 nM (*25*), this approach will not detect large changes in the binding site affinity. To circumvent this limitation, we have extended the vinblastine concentration range by employing a "homologous displacement" assay with a single concentration of [^{3}H]vinblastine (100 nM), as illustrated in Figure 2b. In our hands this meant that concentrations of 1−3 μM vinblastine could be achieved. At 1−3 μM vinblastine, the nonspecific binding represented approximately 40−50% of total binding, but there are difficulties with accurately determining specific binding beyond this proportion, as recently reviewed (*17*). Combining the two assay types into the "mixed homologous saturation assay" produced specific binding data as illustrated in Figure 2c, which produced a $K_d = 42$ nM and a $B_{max} = 57$ pmol/mg. The values were obtained from the best-fit curve, which was the Langmuir isotherm (eq 1) that describes binding to a single site on the protein. Transformation of binding data to the linear Scatchard plot shown in Figure 2d produced a linear relationship, which is also indicative of a single class of binding site for vinblastine on P-gp. However, it has been well demonstrated that analysis of binding data by linear transformation is inaccurate (*16*, *17*, *26*−*28*) and was therefore not further used in the present manuscript.

The data in Figure 3 obtained for [^{3}H]vinblastine binding to P-gp in the absence of nucleotide represent data collected from 10 independent membrane preparations. Curve fitting with eq 1 indicated that the binding capacity was 59 ± 4 pmol/mg with an affinity of 80 ± 19 nM. The data were also fitted with the Adair equation to determine the number of distinct classes of binding site for [^{3}H]vinblastine on P-gp. Equation 1, which describes binding to a single class of binding site, best fitted the experimental data, and the goodness of fit was determined using the *F*-test (*F*-test, $P < 0.05$). This rigorous analysis was used for each mixed homologous saturation assay performed under the various conditions described below.

Effect of Nucleotide Binding on the Drug−P-gp Interaction. What effect, if any, do the early stages of the catalytic cycle have on the vinblastine binding site? To address this, [^{3}H]vinblastine binding was measured in the absence or presence of 2 mM AMP-PNP, and a curve of the average specific binding at each vinblastine concentration is shown in Figure 3a. Previously, we showed that [^{3}H]vinblastine (20 nM) binding was maximally displaced by 2−3 mM AMP-PNP (*10*). By using the mixed homologous saturation assay, it is apparent that the effect of AMP-PNP was to cause a parallel shift to the right in the vinblastine dose−response curve. This shift corresponds to a 9-fold decrease ($P < 0.001$) in the affinity for vinblastine binding from a K_d of 80 ± 18 nM in the absence to $K_d = 731 \pm 20$ nM in the presence of 2 mM AMP-PNP (Table 1). However, the binding capacity of 59 ± 4 pmol/mg observed in controls was not affected by AMP-PNP ($B_{max} = 60 \pm 5$ pmol/mg, Table 1). The dose−response curve provided the best fit for these data as compared to the Adair equation (*F*-test, $P < 0.01$), illustrating that the binding observed in the presence of bound nucleotide triphosphate was still to a single class of site albeit with lower affinity. This switch in binding site affinity to vinblastine was triggered solely by the binding of nucleotide prior to hydrolysis.

What Is the Effect of Nucleotide Hydrolysis on [^{3}H]Vinblastine Binding to P-gp? Having established that the binding of nucleotide at the NBDs triggers a shift in the vinblastine binding site from high to low affinity, we wanted to ascertain whether hydrolysis was required to restore the binding site to high affinity in order to complete a transport cycle. Vanadate trapping was used to stabilize P-gp in the transition state conformation occurring immediately posthydrolysis (*29*). The data in Figure 3b compare the specific binding of [^{3}H]vinblastine to vanadate-trapped and untreated P-gp. Binding to the posthydrolytic P-gp·Mg·ADP·V_i complex displayed a 5.5-fold lower ($P < 0.01$) affinity ($K_d = 446 \pm$

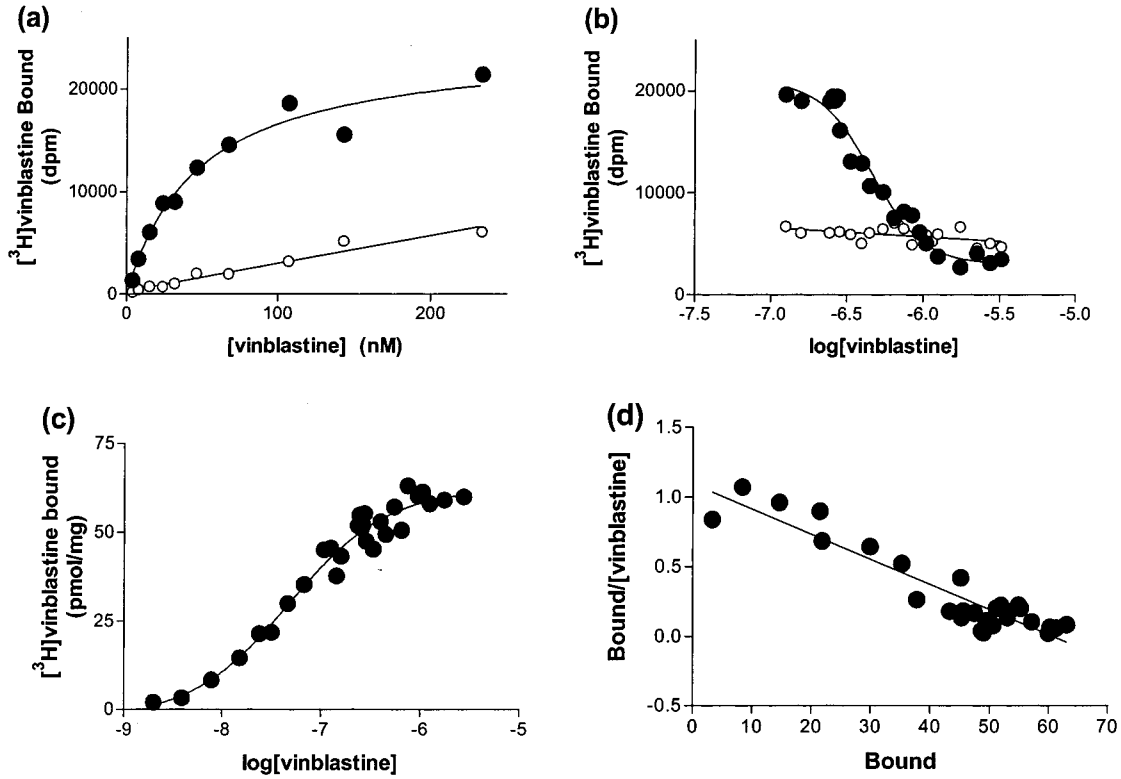

FIGURE 2: Characterization of [^{3}H]vinblastine binding to P-gp in CH^{R}B30 membranes. (a) Saturation isotherm assay. Specific (●) and nonspecific (○) binding of [^{3}H]vinblastine (dpm) expressed as a function of vinblastine concentration from a representative experiment. The different vinblastine concentrations were achieved by adjusting the amount of radiolabeled compound. The curve fitted to the specific binding was obtained from nonlinear regression of eq 1. (b) Homologous displacement assay. Specific (●) and nonspecific (○) binding of [^{3}H]vinblastine (dpm) expressed as a function of vinblastine concentration from a representative experiment. In this case all tubes contained 100 nM [^{3}H]vinblastine, and the total vinblastine concentration varied by addition of unlabeled drug. The curve fitted to the specific binding was obtained from nonlinear regression of eq 5. (c) Mixed homologous saturation assay. The specific binding of [^{3}H]vinblastine to CH^{R}B30 membranes observed in (a) and (b) was converted from dpm to pmol/mg and plotted as a function of vinblastine concentration. The curve fitted to the specific binding was obtained from nonlinear regression of eq 1. (d) Scatchard analysis. The specific binding of [^{3}H]vinblastine to CH^{R}B30 membranes observed in (a) and (b) was converted from dpm to pmol/mg, and a Scatchard plot of the amount bound/[vinblastine] was plotted as a function of the amount bound. Equation 3 was fitted to the data using linear regression.

57 nM, $n = 4$) compared with the untreated control (Table 1). In contrast to the effect on the affinity of binding, the capacity of P-gp to bind [^{3}H]vinblastine was unaltered by vanadate trapping the protein ($B_{max} = 65 \pm 2$ pmol/mg, Table 1). The binding of [^{3}H]vinblastine to P-gp in the presence of bound Mg·ADP·V_i was best fitted by the dose−response equation for a single class of site (F-test, $P < 0.05$). Thus, the hydrolysis of ATP per se does not restore the binding site to a high-affinity state. However, the binding affinity of the vanadate-trapped P-gp appears to represent a pharmacologically distinct state since the K_d value was also significantly different to that found in the presence of AMP-PNP ($P < 0.01$).

How Is High-Affinity Drug Binding Restored during the Catalytic Cycle? To elucidate what signal is required to restore the vinblastine binding site back to its high-affinity configuration, binding of [^{3}H]vinblastine was measured in the presence of the nucleotide diphosphate complex which forms immediately postdissociation of inorganic phosphate. Due to the inherently low-affinity binding of MgADP to P-gp, trapping of the protein was achieved using 8-azidoATP (which is also a substrate for hydrolysis by P-gp) and vanadate, so that the resultant nucleotide diphosphate could be covalently cross-linked to the protein prior to dissociating vanadate. Following dissociation of vanadate, the specific [^{3}H]vinblastine binding was measured using the mixed homologous saturation assay in the presence of bound 8-azidoADP to mimic the ADP-bound form of P-gp (Figure 3c). The binding of [^{3}H]vinblastine was described by a binding capacity of 57 ± 8 pmol/mg and a $K_d = 131 \pm 32$ nM (Table 1). The 1.6-fold higher K_d compared to the control protein was not statistically significant. This suggests that the release of P_i from the posthydrolytic ADP·P_i complex transmits a signal to the TMDs to restore the vinblastine site to its high-affinity conformation.

As a control, the efficiency with which the azido nucleotide diphosphate was cross-linked to the protein in the experiment was determined by assessing the effect of bound 8-azidoADP on the ATP hydrolytic activity of P-gp. There was significant inhibition of drug-stimulated ATP hydrolytic activity in the 8-azidoADP-bound form of the protein when compared to either untreated membranes or membranes subjected to cross-linking conditions in the absence of nucleotide (Figure 4). Thus the lack of any effect of bound 8-azidoADP on [^{3}H]vinblastine binding was not due to inefficient cross-linking of nucleotide. Moreover, there was no effect of treating CH^{R}B30 membranes with UV light on the binding affinity of P-gp for [^{3}H]vinblastine (data not shown). The integrity of P-gp was not affected by the cross-linking procedure, and the protein could be considered to mimic the P-gp·Mg·ADP-bound transition state. Furthermore, investigations by Urbatsch et al. (*30*) and Martin et al. (*10*) have

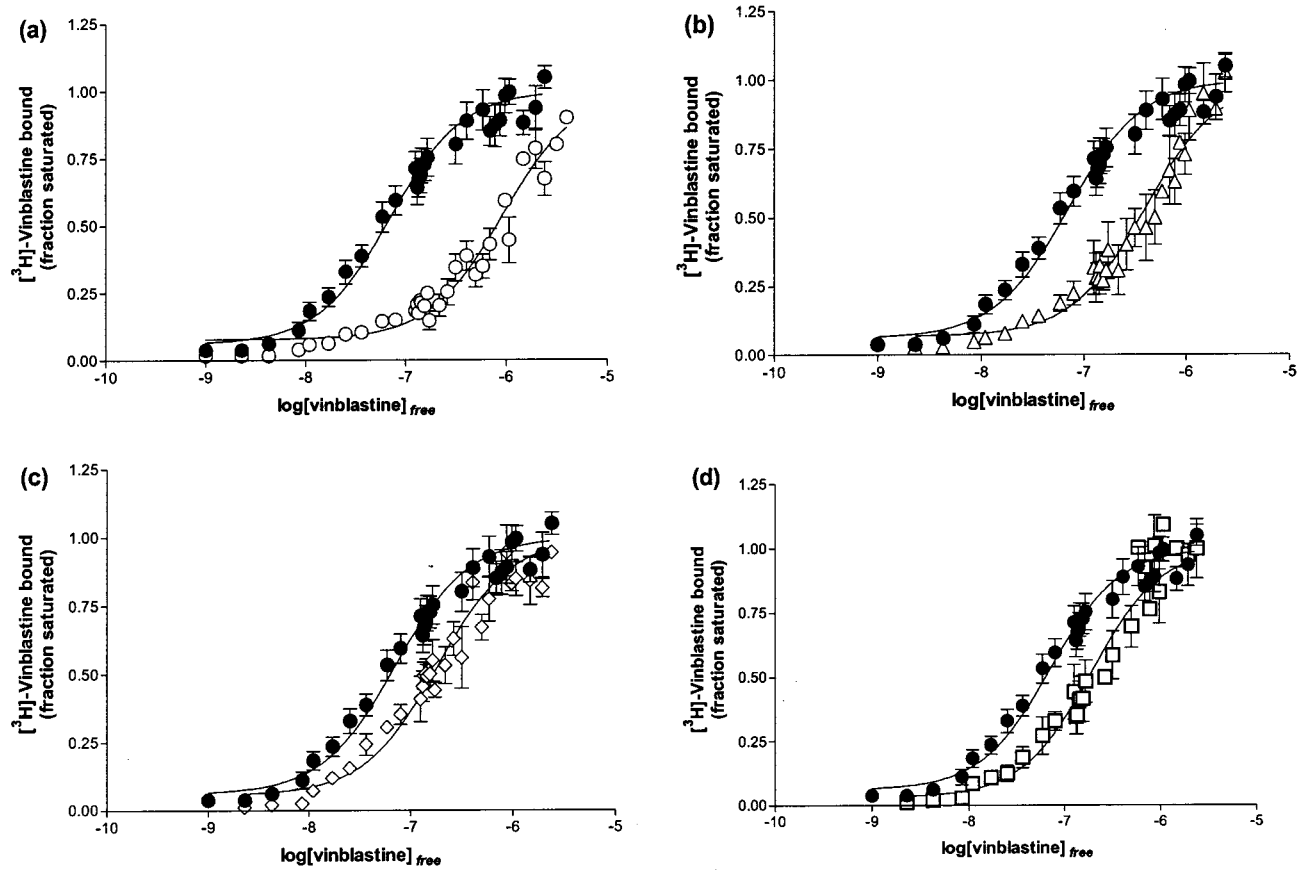

FIGURE 3: Mixed homologous saturation assays were obtained for [^{3}H]vinblastine binding to P-gp under a variety of conditions. (a) Specific binding of [^{3}H]vinblastine to P-gp (15 μg of CH^{R}B30 membrane protein) in the presence (○) or absence (●) of 2 mM AMP-PNP. (b) Specific binding of [^{3}H]vinblastine to P-gp previously trapped in the Mg·ADP·V_i bound state (△). (c) [^{3}H]Vinblastine bound to control (●) and 8-azidoADP labeled (◇) P-gp. (d) Effect of 2 mM AMP-PNP on binding of [^{3}H]vinblastine to P-gp previously cross-linked with 8-azidoADP (□). All values represent mean ± SEM obtained from a minimum of three independent membrane preparations. Specific binding (pmol/mg) was converted to the fraction of B_{max} (fraction saturated), and the data were fitted by nonlinear regression to eq 1.

Table 1: Effect of Distinct Stages of the Catalytic Cycle on the Affinity and Capacity of [^{3}H]Vinblastine Binding[a]

cycle stage	II	III	IV	V	V
nucleotide bound	control	AMP-PNP	ADP + V_i	azidoADP	azidoADP + AMP-PNP
B_{max} (pmol/mg)	59 ± 4	60 ± 5	65 ± 2	57 ± 8	59 ± 14
K_d (nM)	80 ± 18	731 ± 20	446 ± 57	131 ± 32	145 ± 10
n	10	4	4	5	3
P		<0.001	<0.01	NS	NS

[a] Radioligand binding assays measured over a wide range of ligand concentration (0−3000 nM) were used to compare the binding characteristics of [^{3}H]vinblastine in the absence of nucleotide with pre- and postnucleotide hydrolysis stages of the catalytic cycle. Dose−response curves were generated from which a single value of K_d (nM) and B_{max} (pmol/mg) were determined for each different condition as described in Experimental Procedures. The mean ± SEM values were obtained from at least three independent experiments, and the statistical comparisons were performed on the K_d values. The number of observations is defined as *n*. The *P* values were obtained from Student's *t* test for statistical comparisons of mean values to the control (cycle stage I).

extensively characterized conditions under which vanadate dissociates from P-gp, allowing full recovery of both binding and ATPase activities. These conditions were used in the present paper to ensure that the azidoADP cross-linked form of P-gp did not contain bound vanadate.

When Does the Noncatalytically Active NBD Participate in a Transport Cycle? Our data have shown that binding of ATP triggers the conversion of the vinblastine binding site from a high-affinity to a low-affinity state. It is known that only one of the two NBDs of P-gp hydrolyzes ATP during each catalytic cycle. When does nucleotide interact with the noncatalytically active NBD, and what is the consequence of such an event on substrate−P-gp interactions?

P-gp was purified from CH^{R}B30 membranes and reconstituted into liposomes, and the ability of unlabeled 8-azidoATP to prevent the photoaffinity labeling by 8-azido-[α-^{32}P]ATP was determined (Figure 5). Densitometric analysis of photolabeled P-gp showed that 8-azidoATP completely displaced 8-azido[α-^{32}P]ATP labeling, from 47 ± 5 optical density units with an EC_{50} of 16 ± 5 μM. 8-Azido[α-^{32}P]-ATP also labeled P-gp which had been trapped with ADP·V_i. As previously demonstrated, vanadate trapping, and thus labeling with 8-azido[α-^{32}P]ATP, is only possible at a single NBD (*29*). The maximal labeling density was 26 ± 5 optical density units, which corresponded to 50% of the labeling observed for nontrapped protein, and the EC_{50} to displace 8-azido[α-^{32}P]ATP was 58 ± 12 μM.

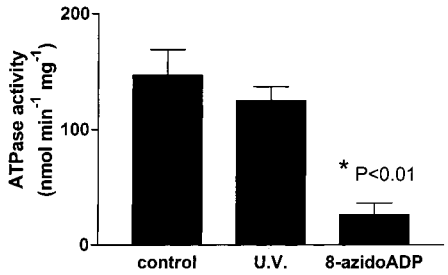

FIGURE 4: Membrane vesicles (1 μg) which had been either untreated or exposed to UV light or UV cross-linking of 8-azidoADP were incubated with 0−2.5 mM Na_2ATP in the presence of 50 μM verapamil over a 20 min period at 37 °C. Dose−response curves plotting ATPase activity as a function of ATP concentration were produced from which values for V_{max} were calculated as described in Experimental Procedures. Values presented represent mean ± SEM of at least three independent experiments.

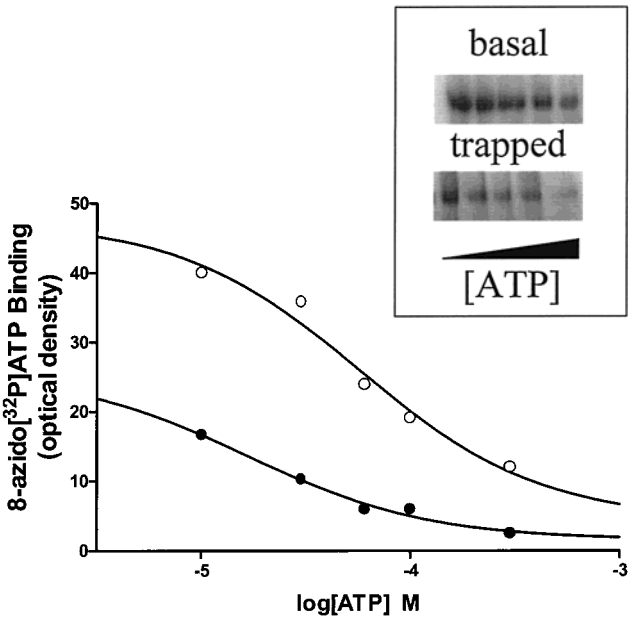

FIGURE 5: Displacement of 8-azido[α-^{32}P]ATP photolabelling of P-gp, purified and reconstituted from CH^RB30 membranes, by increasing unlabeled 8-azidoATP. Labeling was measured by incubating proteoliposomes (8 μg) with 2 μM 8-azido[α-^{32}P]ATP in the presence of increasing unlabeled 8-azidoATP at 37 °C for 15 min. Nucleotide trapping by vanadate was carried out as described in Experimental Procedures. Labeling of nucleotide was measured in trapped P-gp (●) versus untreated P-gp (○). Inset: SDS−PAGE illustrating displacement of 8-azido[α-^{32}P]ATP photolabeling of reconstituted P-gp by unlabeled 8-azidoATP in trapped versus untrapped (basal) protein.

Having demonstrated that ATP can bind to the noncatalytically active NBD when the protein is vanadate trapped, it is reasonable to assume that ATP may still be able to bind at this NBD following dissociation of P_i and while MgADP is still bound at the catalytically active NBD. We have shown that dissociation of P_i causes the conformational change required to restore drug binding sites to high affinity. What effect does binding of ATP have on the drug binding site following dissociation of phosphate but with ADP still bound at the catalytically active NBD? To address this question, an 8-azidoADP cross-linked form of P-gp was generated, and the specific binding of [^{3}H]vinblastine was determined in the presence of 2 mM AMP-PNP (Figure 3d). Under this condition [^{3}H]vinblastine bound to P-gp with an affinity of 145 ± 10 nM and a capacity of 59 ± 14 pmol/mg (Table 1). The lack of any significant AMP-PNP effect on the affinity of [^{3}H]vinblastine binding to the P-gp·Mg·azidoADP complex is in stark contrast to the 9-fold increase in the K_d caused by this nonhydrolyzable nucleotide on untreated P-gp. This suggests that ADP bound at one NBD impairs the ability of ATP bound at the alternate NBD to communicate with the vinblastine binding site.

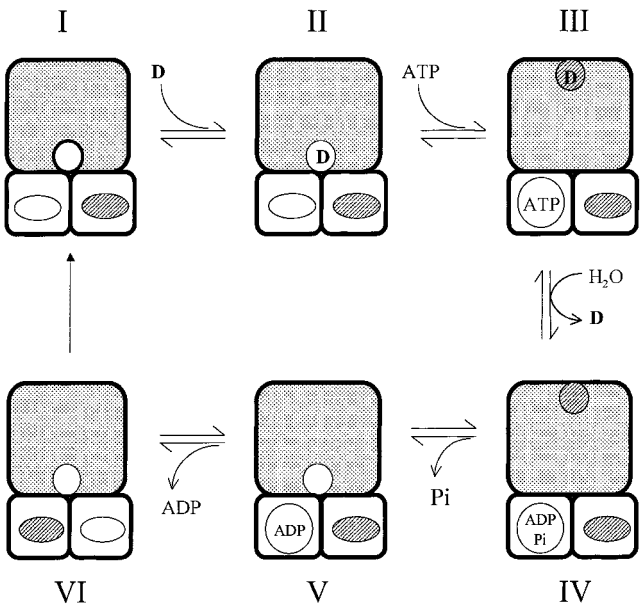

FIGURE 6: On the basis of our study of the characteristics of [^{3}H]vinblastine binding at discrete stages of the catalytic cycle, a model for P-gp-mediated drug transport is presented. The two transmembrane domains are represented by one large shaded square and the NBDs by two small clear squares. The catalytic sites within each NBD are depicted by ellipses; an open ellipse represents open catalytic site conformation and a shaded ellipse closed conformation. Upon nucleotide binding the open catalytic site is depicted by a circle indicating that this is the active NBD, and a shaded ellipse represents the noncatalytic NBD. Stage I depicts the prenucleotide binding state of P-gp where both NBDs are devoid of nucleotide and the drug binding site has a high-affinity inward-facing conformation. The ATP-bound or prehydrolysis state for P-gp is illustrated at stage III, and the drug binding site is now in a low-affinity outward-facing orientation. Stage IV depicts protein following hydrolysis of ATP. Subsequent dissociation of phosphate restores drug binding to an inward-facing high-affinity conformation prior to release of ADP as represented in stage V. Stage VI depicts P-gp following release of ADP from the active catalytic site with possible switching of this site to a passive conformation before entering a new catalytic cycle.

DISCUSSION

The major focus of this study has been to investigate the interplay that occurs between substrate interaction at the TMDs and nucleotide hydrolysis at the NBDs to mediate translocation of drug. With this goal in mind we have systematically carried out a series of radioligand binding experiments to look at the interaction of vinblastine, a cytotoxic drug and transport substrate of P-gp, during discrete stages of the catalytic cycle. We have been able to assess how drug binding site characteristics are altered as P-gp undergoes a transport cycle. On the basis of our findings, a model relating alterations in drug binding at various steps of the catalytic cycle to drug transport has been devised (Figure 6).

Our model shares similarities with that proposed for the bacterial multidrug transporter LmrA (*31*). However, an important difference is that vinblastine bound to two pharmacologically distinct sites on LmrA and that these sites interacted in a cooperative fashion. Hence the authors proposed an alternating two-site cycle of binding affinity changes during each transport cycle. Perhaps a different mechanism for drug recognition and translocation is not unexpected since LmrA is a homodimeric protein whereas P-gp functions in the monomeric state (*32*).

Under basal conditions our model depicts a single class of binding site for vinblastine that displays high affinity for this drug (stage I) and two nucleotide binding domains that participate in an alternating cycle of ATP hydrolysis. The presence of multiple discrete *classes* of binding site (i.e., bind different drugs) on P-gp is now well established (*1*, *3*, *25*, *33*−*35*). It has also been proposed that the sites display overlapping specificities and that a given drug may bind to more than one discrete class of site on P-gp (*36*, *37*). Data supporting this proposal have come from assays that have not *directly* measured drug binding and may reflect allosteric effects of a drug on the binding of another. The complicating effects of such interactions in these assays led us to use the equilibrium binding technique that allows investigation of drug interactions on P-gp by directly measuring the binding event itself. Using this technique,we have previously demonstrated that a given drug, such as vinblastine, interacts with only a single class of site (*1*). In the present investigation we have modified the radioligand binding assay, as described by Rovati (*15*), to use vinblastine concentrations up to 40 times greater than its K_d concentration. The use of such high concentrations enables detection of low-affinity sites of drug interaction on P-gp and to more accurately ascertain the characteristics of vinblastine binding to P-gp (*38*). Modeling of theoretical curves representing single and multiple binding sites to the experimental data in the present investigation demonstrated that vinblastine binding is best described by curves representing interaction at a single class of site on P-gp. What we are unable to determine is whether more than one actual site of a particular class (e.g., capable of binding vinblastine) exists on P-gp. Such a scenario would remain undetected by our analyses only if all of the sites within a class responded identically to nucleotide-induced stimuli.

The next step in our transport cycle model proposes that the binding of nucleotide to the P-gp·VBL complex (stage II) leads to a conformational change resulting in a switch of the vinblastine binding site to a low-affinity state (stage III). It has been generally assumed that the energy generated by hydrolysis of ATP triggers the conformational change in the binding site required to mediate translocation of drug by P-gp. The reduced photoaffinity labeling by [^{125}I]iodoarylazidoprazosin (*11*, *12*, *39*) and impaired binding of [^{3}H]vinblastine and [^{3}H]XR9576 (*10*) to P-gp trapped in a posthydrolytic transition state (stage IV of our model) support this hypothesis. However, investigations involving the vanadate-trapping procedure cannot discriminate between changes occurring due to nucleotide binding and those due to hydrolysis. Our preliminary observations with a nonhydrolyzable nucleotide analogue demonstrated that vinblastine binding was impaired in an early prehydrolytic conformation of P-gp (III in our model) (*10*). The present study extends this hypothesis by establishing that nucleotide binding is associated with a reduction in the affinity of the vinblastine binding site rather than abrogation of its binding. The binding site for the transported drug azidopine has also been demonstrated to undergo a shift to low affinity in the presence of AMP-PNP and ATP-γ-S (*40*). Nucleotide binding, prior to hydrolysis, has also been shown to elicit the conformational changes required to activate/gate the ABC chloride channel CFTR (*41*). Several investigations using fluorescence (*4*, *36*), FTIR spectroscopy (*5*), proteolytic enzyme sensitivity (*8*), and antibody binding (*9*) all demonstrate conformational changes in P-gp prior to any hydrolysis induced by binding of nucleotide. Interestingly, however, the interaction of [^{3}H]XR9576 with P-gp is not affected by AMP-PNP binding (*10*). This lack of effect is presumably related to the nature of the interaction between [^{3}H]XR9576 and P-gp. The binding site itself can be converted to low affinity by nucleotide since P-gp that had previously been trapped in stage IV subsequently displays low affinity for XR9576 (*10*). [^{3}H]XR9576, unlike vinblastine, is a nontransported modulator of P-gp as demonstrated directly using cellular accumulation assays (*25*). This may indicate that modulators such as XR9576 inhibit P-gp-mediated transport by preventing the "trigger" induced by binding of nucleotide to move drug binding sites between conformations.

The different affinities with which [^{3}H]vinblastine binds to P-gp in stages III and IV of the cycle in Figure 6 indicate that they represent distinct conformational states of the protein. This finding is confirmed by evidence from electron microscopy of two-dimensional crystals of P-gp that show distinct structures for vanadate-trapped and AMP-PNP-bound protein (*49*). However, it is not possible to determine their respective roles during the translocation process mediated by P-gp.

In terms of alterations in the vinblastine binding site, we have shown that a second dramatic conformational change is wrought in going from stage IV to stage V in our model. This conformational shift occurs when inorganic phosphate dissociates from the P-gp·ADP·P_i complex, a step that is thought to be associated with the large release of free energy generated by ATP hydrolysis (*42*). Therefore, our data suggest that the energy from hydrolysis is harnessed to restoring the drug binding site to a high-affinity conformation (stage IV → stage V) enabling a subsequent transport event to occur. This is supported by the finding that the dissociation of vanadate (V_i) from the P-gp·ADP·V_i stage (IV) leads to complete recovery of ATP hydrolytic activity and drug (vinblastine and XR9576) binding (*10*, *29*). Moreover, our model proposes that hydrolysis of a single molecule of nucleotide is sufficient to drive the cycling of drug binding sites between high and low affinities. Investigations of P-gp-mediated transport of rhodamine 123 (*43*) and valinomycin (*44*) also demonstrate a coupling ratio of one molecule of ATP hydrolyzed per drug molecule transported. However, a recent investigation implies that a second hydrolytic event is necessary to restore high-affinity binding of [^{125}I]iodoarylazidoprazosin following vanadate trapping in stage IV (*12*). Our results are consistent with previous reports that P-gp completely recovers from vanadate trapping in the absence of added nucleotide or drug (*29*) although the rate of this recovery could be hastened by the addition of ATP. The discrepancy with the findings using the prazosin

analogue may arise from the nature of its physicochemical interaction with P-gp. For example, compared with vinblastine, the modulator XR9576 has a significantly lower dissociation rate (*25*), and the stimulus caused by a second ATP hydrolysis event may increase the rate at which the high-affinity state of its binding site is restored. Alternatively, the discrepancy may be due to the concentration of [^{125}I]iodoarylazidoprazosin used (150-fold less than its K_d) in the investigation (*12*). This is particularly pertinent since the concentration of free drug drives its association with binding sites on a receptor (*38*), and it is possible that if low concentrations are used, the restoration of binding sites to high affinity may take considerably longer.

The model in Figure 6 proposes that the nonhydrolyzing nucleotide binding domain plays a passive role in the first transport cycle/event. Our data demonstrate that ATP may still interact with and bind at this "passive" nucleotide binding domain, yet the alternate site mechanism precludes any simultaneous hydrolytic activity (*45*−*47*). The ability of ABC proteins to simultaneously *bind* nucleotide at both NBDs has also been observed for CFTR (*41*) and the multidrug resistance protein MRP1 (*48*). Can the interaction of ATP to the passive NBD also induce the substrate binding site to undergo the high- to low-affinity conformational change observed earlier in the catalytic cycle? To address this question, we trapped P-gp in stage V by covalently cross-linking with azidoADP. P-gp in this stage of the cycle displayed high-affinity vinblastine binding. However, AMP-PNP binding did not cause a conformational change similar to that seen between stages II and III, indicative of a passive role for the alternate nucleotide binding domain. It is reasonable to speculate that at stage V a second molecule of vinblastine binds to its site, ready to undergo the stage II → stage III conformational change that ultimately leads to translocation of the molecule. We have already shown that a molecule of ATP may also bind to the passive nucleotide binding domain; however, it may only trigger the conformational change once the already bound ADP molecule dissociates (i.e., after stage V). Therefore, our model proposes that each phase of the alternating catalytic cycle is responsible for the movement of a single vinblastine molecule and the initial trigger for this movement is the binding of nucleotide.

ACKNOWLEDGMENT

The authors thank David McIntosh, Tshepo Seekoe, Kenneth Linton, Ian Kerr, and Andrew Taylor for many helpful suggestions and discussions regarding the manuscript.

REFERENCES

1. Martin, C., Berridge, G., Higgins, C. F., Mistry, P., Charlton, P., and Callaghan, R. (2000) *Mol. Pharmacol. 58*, 624−632.
2. Orlowski, S., Mir, L. M., Belehradek, J., and Garrigos, M. (1996) *Biochem. J. 317*, 515−522.
3. Pascaud, C., Garrigos, M., and Orlowski, S. (1998) *Biochem. J. 333*, 351−358.
4. Liu, R., and Sharom, F. J. (1996) *Biochemistry 35*, 11865−11873.
5. Sonveaux, N., Shapiro, A. B., Goormaghtigh, E., Ling, V., and Ruysschaert, J. M. (1996) *J. Biol. Chem. 271*, 24617−24624.
6. Sonveaux, N., Vigano, C., Shapiro, A. B., Ling, V., and Ruysschaert, J. M. (1999) *J. Biol. Chem. 274*, 17649−17654.
7. Wang, G., Pincheira, R., and Zhang, J.-T. (1998) *Eur. J. Biochem. 255*, 383−390.
8. Julien, M., and Gros, P. (2000) *Biochemistry 39*, 4559−4568.
9. Mechetner, E. B., Schott, B., Morse, B. S., Stein, W. D., Druley, T., Davis, K. A., Tsuruo, T., and Roninson, I. B. (1997) *Proc. Natl. Acad. Sci. U.S.A. 94*, 12908−12913.
10. Martin, C., Berridge, G., Mistry, P., Higgins, C., Charlton, P., and Callaghan, R. (2000) *Biochemistry 39*, 11901−11906.
11. Ramachandra, M., Ambudkar, S. V., Chen, D., Hrycyna, C. A., Dey, S., Gottesman, M. M., and Pastan, I. (1998) *Biochemistry 37*, 5010−5019.
12. Sauna, Z. E., and Ambudkar, S. V. (2000) *Proc. Natl. Acad. Sci. U.S.A. 97*, 2515−2520.
13. Kartner, N., Riordan, J. R., and Ling, V. (1983) *Science 221*, 1285−1288.
14. Lever, J. E. (1977) *J. Biol. Chem. 252*, 1990−1997.
15. Rovati, G. E. (1998) *Trends Pharmacol. Sci. 19*, 365−369.
16. Pliska, V. (1995) *J. Recept. Signal Transduction Res. 15*, 651−675.
17. Bylund, D. B., and Murrin, L. C. (2000) *Life Sci. 67*, 2897−2911.
18. Waud, D. R. (1968) *Pharmacol. Rev. 20*, 49−88.
19. Monod, J., Wyman, J., and Changeux, J. P. (1965) *J. Mol. Biol. 12*, 88−118.
20. Chifflet, S., Chiesa, U. T. R., and Tolosa, S. (1988) *Anal. Biochem. 168*, 1−4.
21. Goodno, C. C. (1982) *Methods Enzymol. 85*, 116−123.
22. Callaghan, R., Berridge, G., Ferry, D. R., and Higgins, C. F. (1997) *Biochim. Biophys. Acta 1328*, 109−124.
23. Rothnie, A. R., Soceneantu, L., Theron, D., Martin, C., Berridge, G., Deveaux, P., Higgins, C. F., and Callaghan, R. (2001) *Eur. Biophys. J. 30*, 430−442.
24. Rigaud, J.-L., Levy, D., Mosser, G., and Lambert, O. (1998) *Eur. Biophys. J. 27*, 305−319.
25. Martin, C., Berridge, G., Mistry, P., Higgins, C., Charlton, P., and Callaghan, R. (1999) *Br. J. Pharmacol. 128*, 403−411.
26. Burgisser, E. (1984) *Trends Pharmacol. Sci. 9*, 142−144.
27. Burgisser, E. (1984) *J. Recept. Res. 4*, 357−369.
28. Monot, C., Netter, P., Stalars, M. C., Martin, J., Royer, R. J., and Gaucher, A. (1983) *J. Pharmacol. Sci. 72*, 35−41.
29. Urbatsch, I. L., Sankaran, B., Weber, J., and Senior, A. E. (1995) *J. Biol. Chem. 270*, 19383−19390.
30. Urbatsch, I. L., Sankaran, B., Weber, J., and Senior, A. E. (1995) *J. Biol. Chem. 270*, 19383−19390.
31. van Veen, H. W., Margolles, A., Muller, M.,Higgins, C. F., and Konings, W. N. (2000) *EMBO J. 19*, 2503−2514.
32. Loo, T. W., and Clarke, D. M. (1996) *J. Biol. Chem. 271*, 27488−27492.
33. Ayesh, S., Shao, Y.-M., and Stein, W. D. (1996) *Biochim. Biophys. Acta 1316*, 8−18.
34. Ferry, D. R., Russell, M. A., and Cullen, M. H. (1992) *Biochem. Biophys. Res. Commun. 188*, 440−445.
35. Ferry, D. R., Malkhandi, J. P., Russell, M. A., and Kerr, D. J. (1995) *Biochem. Pharmacol. 49*, 1851−1861.
36. Liu, R., and Sharom, F. J. (1998) *Biochemistry 37*, 6503−6512.
37. Shapiro, A. B., and Ling, V. (1997) *Eur. J. Biochem .250*, 130−137.
38. Kenakin, T. (1997) *Pharmacologic Analysis of Drug-Receptor Interaction*, 3rd ed., Lippincott-Raven, Philadelphia, PA.
39. Dey, S., Ramachandra, M., Pastan, I., Gottesman, M. M., and Ambudkar, S. V. (1997) *Proc. Natl. Acad. Sci. U.S.A. 94*, 10594−10599.
40. Urbatsch, I. L., and Senior, A. E. (1995) *Arch. Biochem. Biophys. 316*, 135−140.
41. Csanady, L., Chan, K. W., Seto-Young, D., Kopsco, D. C., Nairn, A. C., and Gadsby, D. C. (2000) *J. Gen. Physiol. 116*, 477−500.

42. Senior, A. E., Al-Shawi, M. K., and Urbatsch, I. L. (1995) *FEBS Lett. 377*, 285−289.
43. Shapiro, A. B., and Ling, V. (1998) *Eur. J. Biochem. 254*, 189−193.
44. Eytan, G. D., Regev, R., and Assaraf, Y. G. (1996) *J. Biol. Chem. 271*, 3172−3178.
45. Urbatsch, I. L., Sankaran, B., Bhagat, S., and Senior, A. E. (1995) *J. Biol. Chem. 270*, 26956−26961.
46. Senior, A. E., and Bhagat, S. (1998) *Biochemistry 37*, 831−836.
47. Loo, T. W., and Clarke, D. M. (1995) *J. Biol. Chem. 270*, 21449−21452.
48. Hou, Y.-X., Cui, L., Riordan, J. R., and Chang, X.-B. (2000) *J. Biol. Chem. 275*, 20280−20287.
49. Rosenberg, M. F., Velarde, G., Ford, R. C., Martin, C., Berridge, G., Kerr, I., Callaghan, R., Schmidlin, A., Linton, K. J., and Higgins, C. F. (2001) *EMBO J. 20*, 5615−5625.

BI011211Z